# A discrete approximation of Blake & Zisserman energy in image denoising and optimal choice of regularization parameters

Anis Theljani, Zakaria Belhachmi

Received xxxxxxxx; | Revised xxxxxxxxx; | Accepted xxxxxxx

DOI: xxx/xxxx

ARTICLE TYPE

# A discrete approximation of Blake & Zisserman energy in image denoising and optimal choice of regularization parameters.

Anis Theljani[1] | Zakaria Belhachmi[2]

[1]Department of Mathematical Sciences and EPSRC Liverpool Centre for Mathematics in Healthcare, University of Liverpool, Liverpool, United Kingdom

[2]Université de Haute-Alsace, IRIMAS UR 7499 F-68100 Mulhouse and université de Strasbourg, France, F-68100 Mulhouse, France

**Correspondence**

*Zakaria Belhachmi. Email: zakaria.belhachmi@uha.fr

**Summary**

We consider a multi-scale approach for the discrete approximation of a functional proposed by Bake and Zisserman (BZ) for solving image denoising and segmentation problems. The proposed method is based on simple and effective higher order variational model. It consists of building linear discrete energies family which Γ-converges to the non-linear BZ functional. The key point of the approach is the construction of the diffusion operators in the discrete energies within a finite element adaptive procedure which approximate in the Γ-convergence sense the initial energy including the singular parts. The resulting model preserves the singularities of the image and of its gradient while keeping a simple structure of the underlying PDEs, hence efficient numerical method for solving the problem under consideration. A new point to make this approach work is to deal with constrained optimization problems that we circumvent through a Lagrangian formulation. We present some numerical experiments to show that the proposed approach allows us to detect first and second-order singularities. We also consider and implement to enhance the algorithms and convergence properties, an augmented Lagrangian method using the alternating direction method of Multipliers (ADMM).

**KEYWORDS:**

Image restoration - image segmentation - Inverse problems - Regularization procedures - Finite elements.

## 1 | INTRODUCTION

Image denoising and segmentation problems have been intensively studied in the last decades and several approaches based on statistical methods, learning, wavelets or PDEs were developed with variable success have been registered, depending on the nature of the images under consideration (geometric features, textures, …)[1,2,3,4,5,6]. Both the difficulties and the advantages of each method are deeply related to a best handling of small singular sets (edges, corners,…). In the PDEs community, a second-order model, proposed first by Mumford and Shah (M-S)[7], turns out to be among the most successful. It consists of minimising the energy:

$$\frac{\gamma}{2}\int_{\Omega\setminus\Gamma} |\nabla u|^2\, dx + \frac{1}{2}\int_{\Omega} \lambda_0 (u-f)^2 dx + \mathcal{H}^1(S_u), \tag{1}$$

where $u$ is the (reconstructed) image, $f$ the initial image and $S_u$ is the set of the contours of $u$. $\mathcal{H}^1$ denotes the $1-$dimensional Hausdorff measure is the size of $S_u$, which generalizes the length for regular curves. The variational framework, allows for various approximations of the Mumford & Shah functional in both continuous and discrete settings (see[8,9,10,11]. In[8], Ambrosio and

Tortorelli proposed an elliptic approximation on the Sobolev spaces via the $\Gamma$-convergence. In their approach, the discontinuity set $S_u$ is approximated by an auxiliary variable $z$ which plays the role of an indicator function intended to take the value 0 at the edges and 1 in the rest. In [9,10], a discrete approximation of the Mumford-Shah energy were proposed and it is based on a finite element discretization and an adaptive mesh strategy.

However, the Mumford-Shah functional fails to capture the “discontinuities of second kinds", i.e., the set of gradient discontinuity. This limitation produces also some staircasing effect. In order to overcome such shortcomings of the Mumford-Shah functional, Blake and Zisserman (B-Z) [12] proposed a new variational model (1987) which exhibits a second order derivatives by considering the following energy:

$$\int_{\Omega\setminus(S_u\cup S_{\nabla u})} |\nabla^2 u|^2 dx + \xi\mathcal{H}^{n-1}(S_u\cap\Omega) + \beta\mathcal{H}^{n-1}((S_{\nabla u}\setminus S_u))\cap\Omega) + \frac{1}{2}\int_\Omega \lambda_0(u-f)^2\, dx. \tag{2}$$

The previous energy is defined in the class of functions of

$$BV^2(\Omega) = \{v\in BV(\Omega),\ \nabla v\in BV(\Omega)\}\,.$$

It depends on the free discontinuities, free gradient discontinuities and second derivatives of $u$ (see [13,14,15,16] for more details). The discontinuities of $u$ and of $\nabla u$ are “a priori "unknown, hence the associated minimization problem turns out to be essentially non trivial. A challenging problem is how to get effective and suitable numerical schemes for the computation of solutions for Blake-Zisserman energy? In the same spirit of the elliptic approximation of the Mumford-Shah energy, Ambrosio *et al.* (2001) proposed the following functional:

$$\begin{aligned} BZ_\epsilon(u) = \int_\Omega z^2|\nabla^2 u|^2 dx + \int_\Omega (s^2+\sigma)|\nabla u|^2 dx + (\xi-\beta)\int_\Omega \epsilon|\nabla s|^2 + \frac{(s-1)^2}{4\epsilon}dx \\ +\beta\int_\Omega \epsilon|\nabla z|^2 + \frac{(z-1)^2}{4\epsilon}dx + \frac{1}{2}\int_\Omega \lambda_0(u-f)^2 dx, \end{aligned} \tag{3}$$

defined on Sobolev spaces. The minimization of the previous energy acts not only on the restored image $u$ but also on two auxiliary functions: $s$ which is a control function for $\nabla u$ and $z$ which is a control function of the Hessian of $u$, i.e., $\nabla^2 u$ (see [12,17]). Thus, the functional $BZ_\epsilon$ implies a minimization over the variables $(u,s,z)$ of a non-linear PDEs system. Besides, one of the limitation of this method is the dependency on threshold parameters, producing thickness around the edges. But a major shortcoming is the knowledge of the exact constants $\xi$ and $\beta$ the difference of which gives exactly the size $S_u\setminus S_{\nabla u}$ and which is difficult, if not impossible to have a priori.

## CONTRIBUTION AND ORGANIZATION OF THE PAPER

In previous works, we have proposed another approach close to the one followed by [9], based on the construction of a family of discrete energies which converge (in the $\Gamma$-convergence sense) to MS -like functional, i.e. with the length term $\mathcal{H}^1(S_u)$, [18,19]. The method acts essentially with two ingredients: a tight location of the singular set using a posteriori error indicators, and a decreasing of a diffusion function which inhibits the diffusion cross the edges. the method doesn't uses threshold parameters and the length of singular sets is controlled by the Lebesgue measure of the set where the diffusion value is minimal. In this article, we follow this idea and build a $\Gamma$-convergent family of discrete energies which aims to obtain, in the limit, the BZ-energy. We consider the following higher order energy

$$\mathcal{I}(u) = \frac{1}{2}\int_\Omega \beta(x)|\nabla^2 u|^2 dx + \frac{1}{2}\int_\Omega \alpha(x)|\nabla u|^2\, dx + \frac{\lambda_1}{2}\int_\Omega |u-f|^2 dx + \frac{\lambda_2}{2}\int_\Omega |\nabla u - \nabla f_\sigma|^2\, dx, \tag{4}$$

where $0<\alpha_{min}\leq\alpha$, $0<\beta_{min}\leq\beta$. $\nabla^2 u$ is the Hessian matrix of $u$, $\lambda_1>0$, $\lambda_2\geq 0$. The first and the second part in the energy (4) are regularization terms. The third part is a data fidelity term which enforce the solution to be close to the initial image $f$ (in the $L^2$ or $H^1$ norms). We emphasize that under this expression the relevant information on the singularity set $S_u$ and $S_{\nabla u}$ is contained in the diffusion functions $\alpha$ and $\beta$, but the set $S_u\setminus S_{\nabla u}$ is contained in the set $\left\{x\in\Omega;\alpha=\alpha_{min}\Lambda\beta>\beta_{min}\right\}$. We notice also that taking $\lambda_2>0$, adds a term which is not in the initial BZ functional; this term is only added to enhance the gradient of $u$.

In order to solve problem (4), we consider a Lagrangian approach , where we transform our problem in a constrained minimization one, by considering as a variables $u$ and $\mathbf{w}=\nabla u$, this has also the advantage of leading to solve only second order problems. Thus, problem (4) takes the form

$$\min_{u,\mathbf{w}} \mathcal{J}_1(u) + \mathcal{J}_2(\mathbf{w}), \quad \text{subject to} \quad Au + B\mathbf{w} = 0,$$

where $\mathcal{J}_1(\cdot)$ and $\mathcal{J}_1(\cdot)$ are (second order) convex functions, $A$ and $B$ are linear operators (namely $\nabla$ and $I$ the identity). Then, we make an alternating process to solve separately $\mathcal{J}_1(\cdot)$ (with fixed $\beta$ and $\mathbf{w}$) and $\mathcal{J}_2(\cdot)$ (with fixed $u$, $\alpha$). In each step, we perform the adaptive strategy with $\alpha$ and $\beta$ obtained following the method in [20,18,19]. The selection of these functions is performed locally and adaptively – using error indicators and an efficient mesh adaptation –, to decrease with explicit formulae their values close to edges and corners. These considerations lead to an overall approach that is numerically easy, low cost (in the sense that homogeneous regions are coarsed in the meshes), and efficient in determining the singular sets without a priori knowledge except that they have some length.

## E-I

The paper is organized as follows: In section 2, we prove the existence of solution of the minimization problem (4) under a variational mixed formulation and we introduce the Lagrangian formulation. In section 3, we build a family of discrete approximation energies and perform the analysis in the framework of Γ-convergence approach. We give the main algorithm and the a posteriri error indicators which allows us to perform the diffusion coefficients selection that preserves the singular sets for the function and its gradient. In section 4, in order to improve the convergence rate of the algorithm we present an alternative approach to deal the higher order model (4) via an augmented Lagrangian formulation. In particular, we use an ADMM algorithm (alternating direction descent) to enhance the convergence of the Lagrange multiplier variable. In section 5, we present several numerical simulations to show that both singularities of first and second kind are preserved while the diffusion operators act as high order filtering in the homogeneous zones. We give some conclusions and perspectives to the proposed approach.

## 2 | SPLITTING METHOD

The minimization of the energy (4) leads to a fourth-order partial differential equation. In this work, we consider the following constrained optimization problem:

$$\frac{1}{2}\int_\Omega \beta(x)|\nabla \mathbf{w}|^2 dx + \frac{1}{2}\int_\Omega \alpha(x)|\nabla u|^2\, dx + \frac{\lambda_1}{2}\int_\Omega |u-f|^2 dx + \frac{\lambda_2}{2}\int_\Omega |\mathbf{w} - \nabla f_\sigma|^2\, dx, \tag{5}$$

$$w.r.t \quad \nabla u = \mathbf{w}, \tag{6}$$

Thus, the previous optimization problem splits as follows:

$$\min_{(u,\mathbf{w})\in H^1(\Omega)\times \mathbf{H}^1(\Omega)} \mathcal{J}_1(u) + \mathcal{J}_2(\mathbf{w}), \quad \text{subject to (6)} \tag{7}$$

where

$$\begin{cases} \mathcal{J}_1(u) = \dfrac{1}{2}\displaystyle\int_\Omega \alpha(x)|\nabla u|^2 dx + \dfrac{\lambda_1}{2}\int_\Omega |u-f|^2 dx \\ \mathcal{J}_2(\mathbf{w}) = \dfrac{1}{2}\displaystyle\int_\Omega \beta(x)|\mathbf{grad}\,(\mathbf{w})|^2 dx + \dfrac{\lambda_2}{2}\int_\Omega |\mathbf{w} - \nabla f_\sigma|^2 dx \end{cases}$$

and

$$\mathbf{w} = \begin{bmatrix} w_1 \\ w_2 \end{bmatrix} = \begin{bmatrix} \frac{\partial u}{\partial x_1} \\ \frac{\partial u}{\partial x_2} \end{bmatrix}, \quad \mathbf{grad}\,(\mathbf{w}) = \begin{bmatrix} \frac{\partial \mathbf{w}_1}{\partial x_1} & \frac{\partial \mathbf{w}_1}{\partial x_2} \\ \frac{\partial \mathbf{w}_2}{\partial x_1} & \frac{\partial \mathbf{w}_2}{\partial x_2} \end{bmatrix}.$$

**Proposition 1.** The problem (5) admits a unique solution $(u^*, \mathbf{w}^*) \in H^1(\Omega) \times \mathbf{H}^1(\Omega)$

*Proof.* The functional $\mathcal{J}(\cdot,\cdot)$, as a sum of norms, is continuous, strictly convex on $H^1(\Omega)\times\mathbf{H}^1(\Omega)$. In fact, let $(u_1,\mathbf{w}_1), (u_2,\mathbf{w}_2) \in H^1(\Omega)\times\mathbf{H}^1(\Omega)$ such that $(u_1,\mathbf{w}_1) \neq (u_2,\mathbf{w}_2)$ and $\kappa \in ]0,1[$, then we have:

$$\begin{aligned}\kappa\mathcal{J}(u_1,\mathbf{w}_1)+(1-\kappa)\mathcal{J}(u_2,\mathbf{w}_2) \geq \min(\kappa^2,(1-\kappa)^2)\left[\int_\Omega \alpha(x)|\nabla(u_1-u_2)|^2\,dx + \lambda_1\int_\Omega |u_1-u_2|^2\,dx\right]+ \\ \min(\kappa^2,(1-\kappa)^2)\left[\int_\Omega \beta(x)|\mathbf{grad}\,(\mathbf{w}_1-\mathbf{w}_2)|^2\,dx\right]+\lambda_2\int_\Omega |\mathbf{w}_1-\mathbf{w}_2|^2 dx > 0.\end{aligned} \tag{8}$$

We also have that $\mathcal{J}(\cdot,\cdot)$ is coercive and weakly lower semi continuous in $H^1(\Omega)\times\mathbf{H}^1(\Omega)$. Moreover, the feasible set $\mathcal{F} = \{(u,\mathbf{w}) \in H^1(\Omega)\times\mathbf{H}^1(\Omega), \nabla u = \mathbf{w}\}$ of the previous minimization problem is non empty, closed and convex set of $H^1(\Omega)\times\mathbf{H}^1(\Omega)$. Thus, the existence and the uniqueness follows from classical results of calculus of variations[21] □

*Remark 1.* Note that when $\lambda_2 = 0$, we modify in a standard way the space for $\mathbf{w}$, such that $\mathbf{w} \in H^1 \setminus \mathbb{R}$.

### A Lagrangian algorithm

We introduce the space

$$H_0(\mathrm{div},\Omega) = \left\{\mathbf{p} \in (L^2(\Omega))^2; \mathrm{div}\,\mathbf{p} \in L^2(\Omega);\ \mathbf{p}\cdot n = 0,\ \text{on}\,\partial\Omega\right\}.$$

We associate to the primal problem (2.1) − (2.2) the following Lagrangian form:

$$\mathcal{L}_1(u,\mathbf{w},\mathbf{p}) = \mathcal{J}_1(u)+\mathcal{J}_2(\mathbf{w}) - \int_\Omega \mathbf{w}\cdot\mathbf{p} + u\,\mathrm{div}\,\mathbf{p}\,dx, \tag{9}$$

We can show that the there exists a saddle-point $(u^*,\mathbf{w}^*,\mathbf{p}^*) \in H^1\times\mathbf{H^1}\times H_0(\mathrm{div},\Omega)$ of the Lagrangian $\mathcal{L}_1(\cdot)$. In fact, let $\mathcal{Q}$ be the dual functional of $\mathcal{L}_1(\cdot)$, which is defined by the following concave functional:

$$\mathcal{Q}(\mathbf{p}) = \inf_{u\in H^1(\Omega),\mathbf{w}\in\mathbf{H}^1(\Omega)} \mathcal{L}_1(u,\mathbf{w},\mathbf{p})$$

Then, the dual problem consists in solving the following maximization problem:

$$\max_{\mathbf{p}\in H_0(\mathrm{div},\Omega)} \mathcal{Q}(\mathbf{p}). \tag{10}$$

Then, since the constraint convex minimization problem (4) has a unique optimal solution $(u^*;\mathbf{w}^*)$, and the dual concave problem (10) also has an optimal solution $\mathbf{p}^*$, it follows that $(u^*;\mathbf{w}^*;\mathbf{p}^*)$ is a saddle point for $\mathcal{L}_1(\cdot)$.

## 3 | DISCRETE APPROXIMATION AND Γ-CONVERGENCE

In the sequel, we follows the adaptive method proposed in[18,22] for the discrete approximation of Mumford-Shah energy (in the scalar case) and we explain how it can be extended to our case for the the variables $u$, $\mathbf{w}$ and $\mathbf{p}$. Notice that the Lagrangian is not convex in $\mathbf{p}$ and thus this part of the energy should be treated separately within the data term.

### Γ-convergence

In[23], the authors proposed an adaptive approach which is based on two ingredients[22]: the usual mesh adaptation and a "functional" adaptation which consists in choosing locally the diffusion coefficients in order to "cut" high gradients of the computed solution. This approach turns out to be a well suited finite element approximation with a family of discrete energies, in the Γ-convergence sense[24] to the Mumford-Shah functional[7] (see[10] for more details).

For a fixed angle $0 < \theta_0 \leq 2\pi/3$, a constant $c \geq 6$, and for $\epsilon > 0$, let $\mathcal{T}_\epsilon(\Omega) = \mathcal{T}_\epsilon(\Omega;\theta_0;c)$ be the set of all triangulations of $\Omega$ whose triangles $K$ have the following characteristics:

(i) The length of each of the three edges of $K$ is between $\epsilon$ and $\epsilon c$.

(ii) The three angles of $K$ are greater than or equal to $\theta_0$.

Let $V_\epsilon(\Omega)$ be the set of all continuous functions $u : \Omega \longrightarrow \mathbb{R}$ such that $u$ is affine on each triangle $K$ of a triangulation $\mathbb{T} \in \mathcal{T}_\epsilon(\Omega)$. For a given $u$, we define $\mathcal{T}_\epsilon(u) \subset \mathcal{T}_\epsilon(\Omega)$ as the set of all triangulations adapted to the function $u$, i.e., such that $u$ is piecewise affine on $\mathbb{T}$. We consider a non-decreasing continuous function $g_i : [0,+\infty) \longrightarrow [0,+\infty)$, $(i = 1,2)$ such that:

$$\lim_{t\to 0} \frac{g_i(t)}{t} = 1, \ \lim_{t\to+\infty} g_i(t) = g_{i,\infty} < +\infty.$$

(one may take for such $g_i$ a concave regularization of $g(t) = \min(t, g_\infty)$). For any $U = (u, \mathbf{w}) \in (L^p(\Omega))^3$, $(p > 1)$ and $\mathbb{T} \in \mathcal{T}_\epsilon(\Omega)$, following [10,9,20] we consider the finite dimensional minimization problem:

$$G_\epsilon(U) = \min_{\mathbb{T}\in\mathcal{T}_\epsilon(\Omega)} \tilde{G}_\epsilon(U, \mathbb{T}), \tag{11}$$

where

$$\tilde{G}_\epsilon(U,\mathbb{T}) = \begin{cases} \sum_{K\in\mathbb{T}} |K\cap\Omega| \dfrac{1}{h_K} g_1(h_K|\nabla u|^2) + |K\cap\Omega|\dfrac{1}{h_K} g_2(h_K|\nabla \mathbf{w}|^2), & U \in (V_\epsilon(\Omega))^3, \mathbb{T} \in \mathcal{T}_\epsilon(\Omega), \\ +\infty, & \text{otherwise.} \end{cases}$$

When $\epsilon$ goes to zero and provided $\theta_0$ is less than some $\Theta > 0$, we have that $G_\epsilon$ converges, in the $\Gamma$-convergence sense to the functional $G$ given by:

$$G(U) = \begin{cases} \displaystyle\int_\Omega |\nabla u(x)|^2\,dx + |\nabla \mathbf{w}(x)|^2\,dx + g_{1,\infty}\mathcal{H}^1(S_u) + g_{2,\infty}\mathcal{H}^1(S_\mathbf{w}), & U \in (L^2(\Omega)\cap GSBV(\Omega))^3, \\ +\infty, & U \in (L^2(\Omega)\backslash GSBV(\Omega))^3. \end{cases}$$

where $GSBV(\Omega)$ is the space of generalized special functions of bounded variation (see [10,9,20] for details). This means, in particular, that minimizers of $G_\epsilon$ converge to a minimizer of $G$.

*Remark 2.* Notice the following important property that we will use next. If $F : X \longrightarrow [-\infty,+\infty]$ is continuous and $(G_\epsilon)_\epsilon$ $\Gamma$-converges to $G$, then $(F + G_\epsilon)_\epsilon$ $\Gamma$-converges to $F + G$.

*Remark 3.* Notice also that at this stage, the $\Gamma$-limit $G$ is different than BZ energy that we want to approximate as the singular sets $S_u$ and $S_\mathbf{w}$ have no reason to be disjoints.

In the sequel, we better clarify the iterative algorithm used in this work (which mimic the proof of $\Gamma$-convergence), and we will see the role and the way to "compute" the diffusion coefficients $\alpha$ and $\beta$. For this purpose, let $\psi$ be the Legendre-Fenchel transform of $g(t,s) = g_1(t) + g_2(s)$ (concave for both variables). Then, we have $\psi(t,s) = \psi_1(t) + \psi_2(s)$ where $\psi_1$ and $\psi_2$ are the Legendre-Fenchel transforms of $-(g_1)$ and $-(g_2)$, respectively. For a given triangulation $\mathbb{T}_\epsilon$, it is readily checked (from convex analysis arguments) that the minimization of $G_\epsilon$ is equivalent to the minimization problem

$$G'_\epsilon(U, U_1, \mathbb{T}_\epsilon) = \sum_{K\in\mathbb{T}_\epsilon} |K\cap\Omega| \left(\alpha_K|\nabla u|^2 + \frac{\psi_1(\alpha_K)}{h_K}\right) + \sum_{K\in\mathbb{T}_\epsilon} |K\cap\Omega| \left(\beta_K|\nabla \mathbf{w}|^2 + \frac{\psi_2(\beta_K)}{h_K}\right),$$

over all $U = (u,\mathbf{w})$ and $U_1 = (\alpha,\beta)$ where $U \in V_\epsilon(\Omega)$ and $\alpha = (\alpha_K)_{K\in\mathcal{T}_\epsilon(\Omega)}$, $\mathbf{w} \in (V_\epsilon(\Omega))^2$ and $\beta = (\beta_K)_{K\in\mathcal{T}_\epsilon(\Omega)}$, piecewise constant on each $K \in \mathcal{T}_\epsilon$.

Now, the minimization over each $\alpha$ and $\beta$ which may be explicitly computed by:

$$\alpha_K = g'_1(h_K|\nabla u|^2) \text{ and } \beta_K = g'_2(h_K|\nabla \mathbf{w}|^2). \tag{12}$$

Then, the choice of $\alpha$ and $\beta$ depends on the functions $g_1$ and $g_2$ and may be computed analytically without solving any PDE. An example of such choices could be given by :

$$g_i(t) = \frac{2g_{i,\infty}}{\pi}\arctan\left(\frac{\pi\, t}{2g_{i,\infty}}\right),$$

which produces smoothly decreasing sequences $\alpha$ and $\beta$ (as the inverse of the magnitude of the respective gradients squared). Whereas, the minimizers $(u,\mathbf{w})$ solve, up to the data terms,

$$\mathcal{R}(u,\mathbf{w}) = \sum_{K\in\mathbb{T}_\epsilon} \int_{K\cap\Omega} \alpha_K|\nabla u|^2\,dx + \sum_{K\in\mathbb{T}_\epsilon} \int_{K\cap\Omega} \beta_K|\nabla \mathbf{w}|^2\,dx \tag{13}$$

To complete the Γ-convergence analysis, let us denote the fidelity term of the Lagrangian by

$$\Phi(U,\mathbf{p};f) = \frac{\lambda_1}{2}\int_\Omega |u-f|^2 dx + \int_\Omega |\mathbf{w}-\nabla f_\sigma|^2 dx - \int_\Omega \mathbf{w}\cdot\mathbf{p} + u\,\mathrm{div}\mathbf{p}\,dx.$$

It is readily checked that $\Phi$ is continuous in $(L^2(\Omega))^3 \times H_0(\mathrm{div},\Omega)$, hence using remark -2, and Γ-convergence of the sequence $G_\epsilon$ to $G$, yields:

**Proposition 2.** Let $f$ be a given function in $L^2(\Omega)$ and $\epsilon > 0$ be a positive parameter. Then the sequence of functionals $(G_\epsilon(\cdot) + \Phi(\cdot,\cdot;f))_\epsilon$, Γ-converges for $\epsilon \longrightarrow 0$. $(G(\cdot) + \Phi(\cdot,\cdot;f))$.

*Remark 4.* The Lagrange multiplier $\mathbf{p}$ in the algorithm makes the data term also dependent on $\epsilon$. However, due to the continuity of $\Phi$, for this third variable, in $H(\mathrm{div},\Omega)$ this dependance does not affect the Γ-convergence of $G_\epsilon + \Phi$. More we precisely, we write $\Phi(.,\mathbf{p}_\epsilon)$, as $\Phi(.,\mathbf{p})$ plus $(\Phi(.,\mathbf{p}) - \Phi(.,\mathbf{p}_\epsilon))$ and use the strong convergence of the last term and the remark 2.

To conclude this section, let us interpret in term of a PDE the Γ-limit of each functional $G$, i.e., corresponding to $u$ and $\mathbf{w}$. The minimizers $(u_\epsilon,\mathbf{w}_\epsilon)$ converge to a minimum $(u,\mathbf{w})$ of $G$ while $(\alpha_\epsilon)$, respectively $(\beta_\epsilon)$, converges to $1_{\Omega\setminus S_u}$, respectively $1_{\Omega\setminus S_\mathbf{w}}$. The singular sets are identified as the sets where $\lim_{\epsilon\longrightarrow 0}\alpha_\epsilon = 0$ for $S_u$, respectively $\lim_{\epsilon\longrightarrow 0}\beta_\epsilon = 0$ for $S_\mathbf{w}$. Notice that the two singular sets are not necessarily disjoints. However, the Hausdorff measure of each set is bounded (tightly) by the Lebesgue measure of the corresponding sets $\{\alpha = \alpha_{min}\}$, respectively $\{\beta = \beta_{min}\}$. Moreover, the Hausdorff measure of the set $S_{\nabla u}\setminus_{S_u}$ is then controlled by $|\{\alpha > \alpha_{min}, \text{ and } \beta = \beta_{min}\}|$. The constants in the BZ functional (or its elliptic regularization) are obtained directly from the data and not chosen a priori.

### Alternate descent algorithm and adaptive approach

Following the method in [20,18], we consider an alternate descent minimization scheme over $(u,\mathbf{w},\mathbf{p})$, $\alpha$, $\beta$ and $\mathbb{T}_\epsilon$ which reads:

$$G'_\epsilon(U,U_1,\mathbb{T}_\epsilon) + \Phi(U_\epsilon,\mathbf{p}_\epsilon;f), \tag{14}$$

The alternate minimization is combined with an adaptive algorithm to approximate B-Z energy, see also [22]. Mainly, we use mesh and "functional" adaptation which consists in choosing locally the diffusion coefficients $\alpha$ and $\beta$ in order to "cut" high gradients of the computed solution $u$ and its gradient $\mathbf{w}$. More precisely, we consider the following algorithm

**Algorithm 1** MINIMIZATION METHOD:

1. Initialization: choose $U_0 = (u_0,\mathbf{w}_0,\mathbf{p}_0)$, $\alpha_0$ and $\beta_0$.
2. Iterations: for fixed $\alpha^k$ and $\beta^k$, find $U^{k+1} = (u^{k+1},\mathbf{w}^{k+1}) \in V_\epsilon(\Omega)^3$ and $\mathbf{p}^{k+1} \in V_\epsilon(\Omega)^2$, solution of problem (13).
3. with $U^{k+1}$ and $\mathbf{p}^{k+1}$ fixed:
   a) Update $\mathbb{T}_\epsilon$ with mesh refinement step (in our case using the metric adaptation with FreeFem++).
   b) Perform a local choice of $\alpha(x)$ and $\beta(x)$ on $\mathcal{T}_h^{k+1}$ to obtain new functions $\alpha_{k+1}$ and $\beta_{k+1}$. (using a posteriori error indicators).
4. Go to step (1) until convergence.

The step $a$), plays the role of minimization over a class of triangulations $\mathcal{T}_\epsilon$, and allows us to obtain a tight location of the singular sets as the residual error indicator is high (or equivalently with the metric adaptation). This means exactly that this locations are the candidate to contain the singularities. We emphasize that we obtain also an approximate solution to problem (14).

For a given $u$ and $\mathbf{w}$ and $T_\epsilon$, the step b) will consists in decreasing the diffusion parameters. Contrary to the scalar case, when a part of the singular set is located with the step $a$) we don't know whether this part is in $S_u$ or $S_\mathbf{w}$ or both. Thus, to perform this step, we first consider the following local error indicators

$$\eta_K = \alpha_K^{\frac{1}{2}}\|\nabla u_h\|_{L^2(K)} \quad\text{and}\quad \eta'_K = \beta_K^{\frac{1}{2}}\|\nabla w_h\|_{L^2(K)}, \tag{15}$$

to decide which parameter ($\alpha$, $\beta$ or both) we decrease. The change in the intensity of the image, respectively the brightness, indicate the set $S_u$, respectively $S_{\mathbf{w}}$. Thus we may know which parameter to change. The map of the above errors indicator allows us to update locally $\alpha$ and $\beta$ on each triangle $K$ using either the formula (12), or the following one (fast decreasing)[20,18] and which is given by

$$\alpha_K^{k+1} = \max\left(\frac{\alpha_K^k}{1+\kappa\left(\frac{\eta_K}{\|\eta\|_\infty} - 0.1\right)^+}, \alpha_{thr}\right),$$

where $\alpha_{thr}$ is a threshold parameter and $\kappa$ is a coefficient chosen to control the rate of decrease in $\alpha$, $u^+ = \max(u, 0)$. The same formula is used to update the function $\beta(x)$ and where $\eta$ is replaced by $\eta'$. Notice that equivalently, we can use the residual errors indicators related to the discrete $u$ and $\mathbf{w}$ subproblems.

Let us gives the details for the step 2. of the algorithm

### The $u$-subproblem

For $\alpha_K$, $\mathbf{w}^k$ and $\mathbf{p}^k$ fixed, the $u$-subproblem is quadratic and consists in solving the following minimization problem:

$$\min_{u\in H^1(\Omega)}\{\sum_{K\in\mathbb{T}_\epsilon}\int_{K\cap\Omega}\alpha_K|\nabla u|^2\,dx + \Phi(U,\mathbf{p};f)\} \tag{16}$$

The minimizer $u^{k+1}$ satisfies the following first-order optimality condition

$$\begin{cases} -\Delta_\alpha u^{k+1} + \lambda_1 u^{k+1} = \lambda_1 f - \mathrm{div}\mathbf{p}^k, & \text{in } \Omega, \\ \frac{\partial u^{k+1}}{\partial n} = 0, & \text{in } \Omega, \end{cases}$$

### The $w$-subproblem

For a fixed $u^{k+1}$, $\beta_K$ and $\mathbf{p}^k$, the $\mathbf{w}$-subproblem consists in solving the following minimization problem:

$$\min_{\mathbf{w}\in\mathbf{H}^1(\Omega)}\{\sum_{K\in\mathbb{T}_\epsilon}\int_{K\cap\Omega}\beta_K|\nabla\mathbf{w}|^2\,dx + \Phi(U,\mathbf{p};f)\} \tag{17}$$

which clearly admits a unique solution $\mathbf{w}^{k+1}$ which fulfils:

$$\begin{cases} -\Delta_\beta \mathbf{w}^{k+1} + \lambda_2 \mathbf{w}^{k+1} = \lambda_2 \nabla f - \mathbf{p}^k, & \text{in } \Omega, \\ \frac{\partial \mathbf{w}^{k+1}}{\partial n} = 0, & \text{in } \Omega, \end{cases}$$

### The $p$-subproblem

The multiplier $\mathbf{p}$ updates linearly as follows: for a given parameter $\tau$ (small)

$$\mathbf{p}^{k+1} = \mathbf{p}^k + \tau\,(\mathbf{w}^{k+1} - \nabla u^{k+1}). \tag{18}$$

*Remark 5.*

1. The existence of solutions of $u$- and $\mathbf{w}$- problems follows from standard techniques of calculus of variations. In fact, it is readily checked by direct calculation that the functional to be minimized are strictly convex, coercive and weakly lower semi-continuous.
2. Notice that problems (16) and (17) may be solved in parallel to accelerate the convergence.
3. The role of $\lambda_2 > 0$ appears clearly at this step to deal with a “non degenerate" Neumann problem.

## 4 | AUGMENTED LAGRANGIAN FORMULATION AND ALTERNATING DIRECTIONS METHOD OF MULTIPLIERS (ADMM)

In order to enhance the quality and the cost of the numerical computations, we use the Augmented Lagrangian formulation, which will be solved using the alternating directions method of multipliers (ADMM). The ADMM is one of the most extensively used algorithms to solve constrained optimization problems, particularly for augmented Lagrangian formulations (see[25,26,27,28] and the references therein).

In our case, we associate to the primal problem (2.1) – (2.2) the following augmented Lagrangian form:

$$\mathcal{L}_\rho(u,\mathbf{w},\mathbf{p}) = \sum_{K\in\mathbb{T}_\epsilon}\int_{K\cap\Omega}\left(\alpha_K|\nabla u|^2 + \beta_K|\nabla\mathbf{w}|^2 - \mathbf{w}\cdot\mathbf{p} + u\,\mathrm{div}\mathbf{p} + \frac{\rho}{2}|\mathbf{w}-\nabla u|^2\right)dx \tag{19}$$

$$= \sum_{K\in\mathbb{T}_\epsilon}\int_{K\cap\Omega}\left((\alpha_K + \tfrac{\rho}{2})|\nabla u|^2 + \beta_K|\nabla\mathbf{w}|^2 + \tfrac{\rho}{2}\mathbf{w}^2 - \mathbf{w}\cdot(\mathbf{p}+\rho\nabla u) + u\,\mathrm{div}\mathbf{p}\right)dx \tag{20}$$

for $\rho > 0$ (usually $\rho = 1$). The ADMM iterations consists in minimizing $\mathcal{L}_\rho(\cdot,\cdot,\mathbf{p})$ with respect to one variable and keeping the other fixed. The Lagrange multiplier $\mathbf{p}$ is up dated at each step in the algorithm and takes the same form (18) as for the classical Lagrangian method. The only change comparing to Algorithm is the $u$ and $\mathbf{w}$ subproblems. The overall algorithm consists in the following steps:

**Algorithm 2** ADMM ALGORITHM

Given $\rho,\ \alpha,\ \beta,\ f$.
Starting guess: $u^0 \in H^1(\Omega)$, $\mathbf{p}^0 \in H_0(\mathrm{div}\,\Omega)$ and $\mathbf{w}^0 \in \mathbf{H}^1(\Omega)$.
For $k = 0, 1, 2, \cdots$ until convergence:

1. Update $u^{k+1}$ by $u^{k+1} =\ \arg\min_u \mathcal{L}_\rho(u,\mathbf{w}^k,\mathbf{p}^k)$.
2. Update $\mathbf{w}^{k+1}$ by solving $\mathbf{w}^{k+1} =\ \arg\min_{\mathbf{w}} \mathcal{L}_\rho(u^k,\mathbf{w},\mathbf{p}^k)$.
3. Update $p^{k+1}$ by solving $\mathbf{p}^{k+1} = \mathbf{p}^k + \rho(\mathbf{w}^{k+1} - \nabla u^{k+1})$.

In the new formulation, problems (16) and (17) are replaced by

$$\begin{cases} -\Delta_{\alpha+\frac{\rho}{2}} u^{k+1} + \lambda_1 u^{k+1} = \lambda_1 f - \rho\mathrm{div}\ \mathbf{w}^k - \mathrm{div}\mathbf{p}^k, & \text{in } \Omega,\\ \frac{\partial u^{k+1}}{\partial n} = 0, & \text{in } \Omega, \end{cases}$$

and

$$\begin{cases} -\Delta_\beta \mathbf{w}^{k+1} + \lambda_2\mathbf{w}^{k+1} + \rho\mathbf{w}^{k+1} = \lambda_2\nabla f + \rho\nabla u^{k+1} - \mathbf{p}^k, & \text{in } \Omega,\\ \frac{\partial \mathbf{w}^{k+1}}{\partial n} = 0, & \text{in } \Omega. \end{cases}$$

### The convergence of the ADMM algorithm

There are many convergence results for ADMM discussed in the literature [29,30,31]. The convergence is guaranteed if the following assumptions are satisfied.

- Energies $\mathcal{J}_1(\cdot)$ and $\mathcal{J}_2(\cdot)$ are convex, closed and proper.
- The augmented Lagrangian $\mathcal{L}_\rho$ admits a saddle point $(u^*,\mathbf{w}^*,\mathbf{p}^*) \in H^1\times\mathbf{H^1}\times H_0(\mathrm{div},\Omega)$.

The first assumption is satisfied as each of the $u$- and $\mathbf{w}$-subproblems admits a unique solution. For the second assumptions, we can show that the there exists a unique saddle-point $(u^*,\mathbf{w}^*,\mathbf{p}^*) \in H^1\times\mathbf{H^1}\times H_0(\mathrm{div},\Omega)$ of the augmented Lagrangian $\mathcal{L}_\rho$. In fact, any saddle-point of the augmented Lagrangian $\mathcal{L}_\rho(\cdot)$ is also a saddle-point of the Lagrangian $\mathcal{L}_1(\cdot)$ in (9), which has a unique saddle point.

*Remark 6.* The use of the ADMM seems to enforce the diffusivity on the function $u$, which may cause loosing its singularities set. Moreover, the analysis of the $\Gamma$-convergence is questionable in the new formulation. To keep the adaptive algorithm able to detect the singularities sets of $u$, we set a new diffusivity function

$$\alpha_n(x) = \alpha(x) + \tfrac{\rho}{2}.$$

Then, we adapt the function $\alpha$ using the same formula and the we rescale it into the interval $[\alpha_{min} - \frac{\rho}{2}, \alpha_{max} - \frac{\rho}{2}]$. Thus, we will be able to detect singularities from the adaptation and the new diffusivity fulfils $0 < \alpha_{min} \le \alpha_n(x) \le \alpha_{max}$, which guarantees the well-posedness of the $u$- problem.

## 5 | NUMERICAL EXAMPLES

In this section, numerical experiments are conducted on images that are corrupted by Gaussian noise. We test the proposed model for first- and second-order discontinuities detection. For the denoising task, we compare our approach with the total variation model (**TV**)[4,2] and a high-order model that we call **HOM**, which corresponds the energy (4) for $\alpha(\cdot) \equiv \beta \equiv (\cdot) = 1$. The original image were corrupted with Gaussian noise having zero mean and different standard deviations, i.e., between 10 and 15.

### Edge detection

In Fig 1 , we test proposed model for $\beta \neq 0$ and $\beta = 0$ for edge detection. We note that the case $\beta = 0$ corresponds to the discrete approximation of the Mumford-Shah energy[20,9]. The values of the functions $\alpha$ and $\beta$ are 1 (white) on homogeneous areas and they are 0 (black) in correspondence of the edges of $u$ and $\mathbf{w} \approx \nabla u$. It is clear the map $\alpha$ is unable to detect the gradient discontinuity. These are regions where $u$ is continuous while $\nabla u$ is discontinuous. The output map $\beta$ of our approach is given by meaningful boundaries corresponding to the discontinuity set of its first derivatives.

### Lagrangian vs Augmented Lagrangian

In Figure 2 , we show the result of the proposed model, solved using the Lagrangian and ADMM, respectively. for both approaches, We display the denoised images, the Lagrange multiplier $\mathbf{p} = (p_1, p_2)$ and the final mesh. The results of both approaches look visually similar, however, the ADMM is much faster for solving the model (5)-(6).

### Image denoising and edges detection

In Figure 3 , we test the proposed model, solved by ADMM, in denoising a satellite image which has some fine structures, correspond to the roads. We show the denoised image, the maps of $\alpha$ and $\beta$. The function $\alpha$ maps the discontinuity of $u$ and the function $\beta$ which maps the discontinuities of $\mathbf{w}$, i.e., approximates the gradient of $u$. Form the map of $\beta$, it clear that latter suitable in detecting fine structures. We also test the model in denoising a medical image, which contains some smooth regions and edges. In these regions, the gradient of the image should discontinuous and they can seen in the map of $\beta$.

### Medical image denoising and edges detection

In the last example, we give in Figure 4 the results obtained with the proposed model solved with the Lagrangian and with ADMM for medical images. We present the plot of $\alpha$ and $\beta$ and the final mesh. This example show the efficiency of the method for medical images where in addition to the variety of fine structures to be detected, the high resolution of the images should also be considered.

We compare the proposed model with the total variation (**TV**) and the high-order (**HOM**) models. In Figure 5 , we display the restored image we give the PSNR values, which confirm that the proposed model can deliver better denoising quality than the other models. We also display the diffusion functions $\alpha$ and $\beta$ which indicates regions that approximate the discontinuity sets of $u$ and $\nabla u$, i.e., $S_u$ and $S_{\nabla u}$, respectively.

## 6 | CONCLUSION

In this paper, we proposed a novel variational model with the good performance such as the alleviation of the staircase effect and the preservation of the edges. By using an alternative approach, we obtain two simple subproblems, acting for alternatively for the solution $u$ and its first order derivatives $\nabla u$. To solve these subproblems, the ADMM algorithm was used in the numerical computation. The use of the ADMM allowed as to see the initial model, which is of high order, as two first-order variational models with unknowns $u$ and $\nabla u$. Then, we performed an adaptive strategy based on the objective selection of the regularization parameters appeared in both energies and mesh adaptation techniques. Analysing the proposed algorithm using $\Gamma$-convergence tools draw connections with the Blake and Zisserman energy. The numerical experiments have demonstrated the effectiveness of our proposed method.

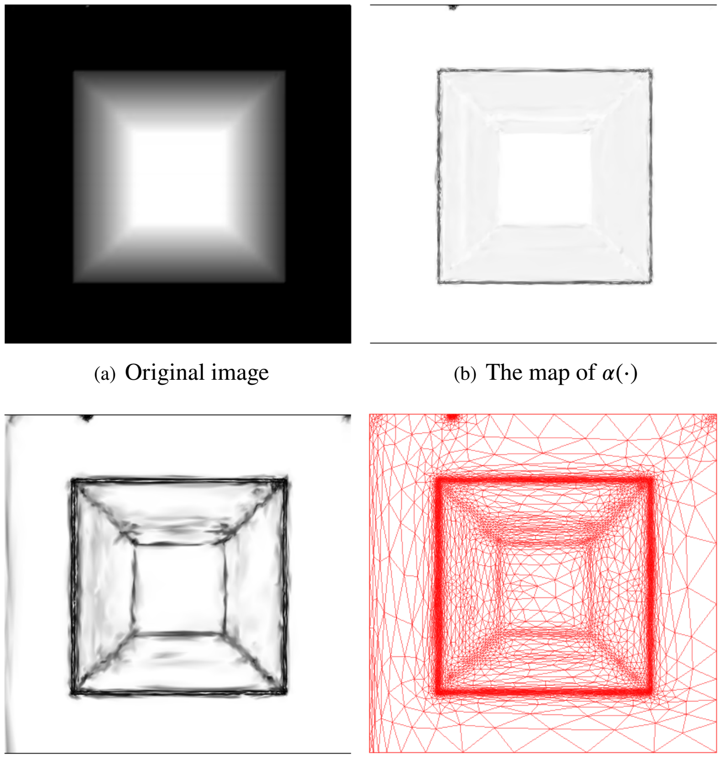

(a) Original image

(b) The map of $\alpha(\cdot)$

(c) The map of $\beta(\cdot)$

(d) The adapted mesh

**FIGURE 1** Example of first- and second-order discontinuities detection using our model

## References


1. Theljani Anis, Belhachmi Zakaria, Moakher Maher. High-order anisotropic diffusion operators in spaces of variable exponents and application to image inpainting and restoration problems. *Nonlinear Analysis: Real World Applications.* 2019;47:251–271.

2. Blomgren Peter, Chan Tony F, Mulet Pep, Wong Chak-Kuen. Total variation image restoration: numerical methods and extensions. In: :384–387, IEEE; 1997.

3. Chan Tony F, Esedoglu Selim, Nikolova Mila. Algorithms for finding global minimizers of image segmentation and denoising models. *SIAM journal on applied mathematics.* 2006;66(5):1632–1648.

4. Vese Luminita A, Osher Stanley J. Image denoising and decomposition with total variation minimization and oscillatory functions. *Journal of Mathematical Imaging and Vision.* 2004;20(1-2):7–18.

5. Blomgren Peter, Chan Tony F. Color TV: total variation methods for restoration of vector-valued images. *IEEE transactions on image processing.* 1998;7(3):304–309.

6. Lu Wenqi, Duan Jinming, Qiu Zhaowen, Pan Zhenkuan, Liu Ryan Wen, Bai Li. Implementation of high-order variational models made easy for image processing. *Mathematical Methods in the Applied Sciences.* 2016;39(14):4208–4233.

7. Mumford David, Shah Jayant. Optimal approximations by piecewise smooth functions and associated variational problems. *Communications on pure and applied mathematics.* 1989;42(5):577–685.

8. Ambrosio L., Tortorelli M.. Approximation of functional depending on jumps by elliptic functional via Γ-convergence. *Comm. Pure Appl. Math..* 1990;43:999–1036.

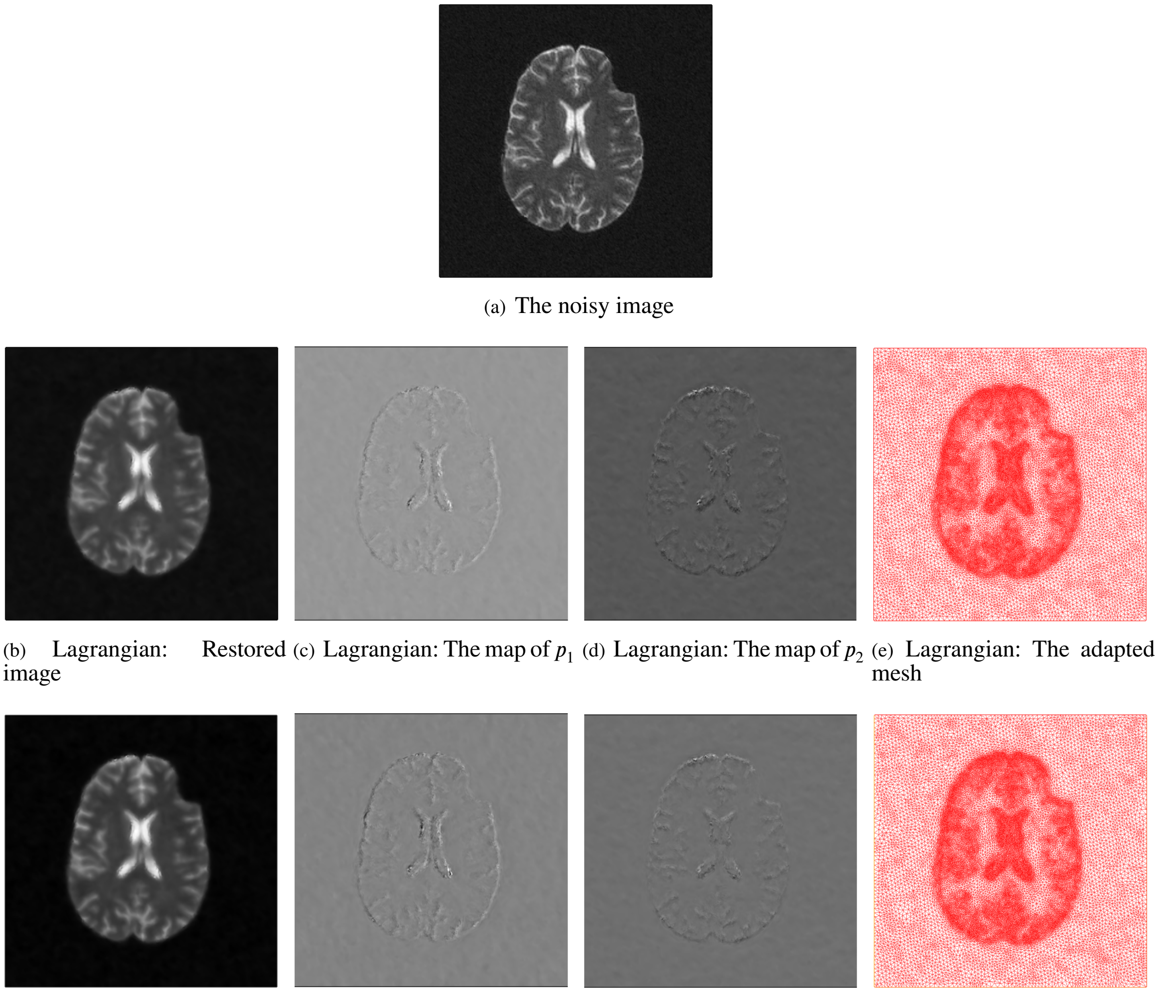

(a) The noisy image

(b) Lagrangian: Restored image (c) Lagrangian: The map of $p_1$ (d) Lagrangian: The map of $p_2$ (e) Lagrangian: The adapted mesh

(f) Augmented Lagrangian: Restored image (g) Augmented Lagrangian: The map of $p_1$ (h) Augmented Lagrangian: The map of $p_2$ (i) Augmented Lagrangian: The adapted mesh

**FIGURE 2** Comparison between the Lagrangian and the augmented Lagrangian. Both approaches gives similar results. However, solving the augmented Lagrangian needs less iteration than the Lagrangian because of the ADMM.


9. Chambolle A., Bourdin B.. Implementation of an adaptive finite-element approximation of the Mumford-Shah functional. *Numer. Math.*. 2000;85(4):609–646.

10. Chambolle A., Maso G. Dal. Discrete approximation of the Mumford-Shah functional in dimension two. *M2AN Math. Model. Numer. Anal.*. 1999;33(4):651–672.

11. Braides A, Dal Maso G. Non-local approximation of the Mumford-Shah functional. *Calculus of Variations and Partial Differential Equations.* 1997;5(4):293–322.

12. Blake A., Zisserman A.. *Visual reconstruction*. Cambridge, MA, USA: MIT Press; 1987.

13. Carriero Michele, Leaci Antonio, Tomarelli Franco. A second order model in image segmentation: Blake & Zisserman functional. In: Springer 1996 (pp. 57–72).

14. Carriero Michele, Leaci Antonio, Tomarelli Franco. Strong minimizers of Blake & Zisserman functional. *Annali della Scuola Normale Superiore di Pisa-Classe di Scienze.* 1997;25(1-2):257–285.

15. Braides Andrea, Defranceschi Anneliese, Vitali Enrico. A compactness result for a second-order variational discrete model. *ESAIM: Mathematical Modelling and Numerical Analysis.* 2012;46(2):389–410.

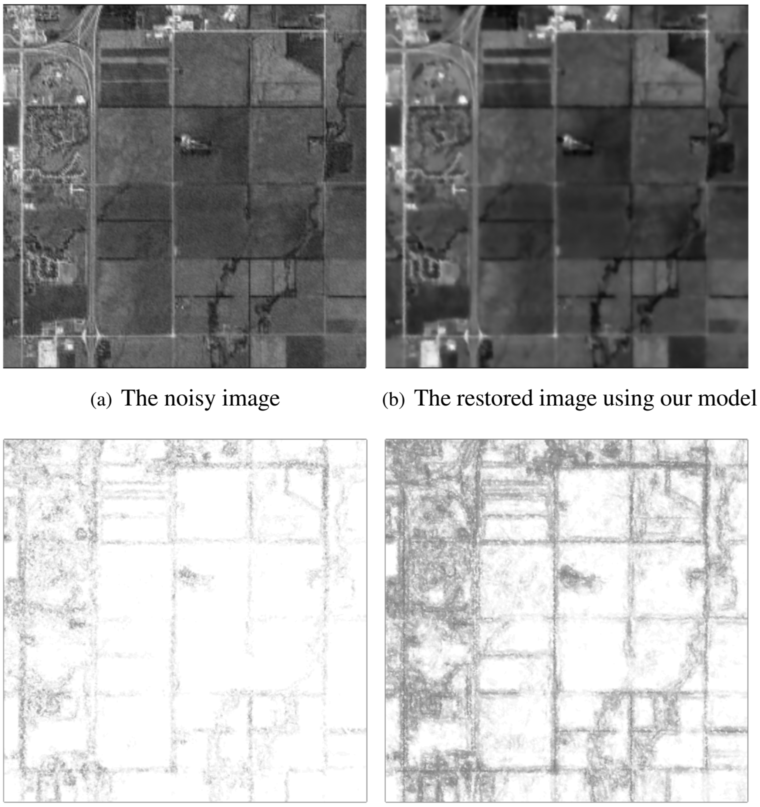

(a) The noisy image (b) The restored image using our model

(c) The map of $\alpha(\cdot)$ (d) The map of $\beta(\cdot)$

**FIGURE 3** Example of denoising and detection of thin structures (roads) using our model. The coefficient $\beta(\cdot)$ is clearly more efficient than $\alpha(\cdot)$ for this task.


16. Ambrosio Luigi, Faina Loris, March Riccardo. Variational approximation of a second order free discontinuity problem in computer vision. *SIAM Journal on Mathematical Analysis.* 2001;32(6):1171–1197.

17. Zanetti Massimo, Ruggiero Valeria, Jr Michele Miranda. Numerical minimization of a second-order functional for image segmentation. *Communications in Nonlinear Science and Numerical Simulation.* 2016;36:528–548.

18. Theljani Anis, Belhachmi Zakaria, Kallel Moez, Moakher Maher. A multiscale fourth-order model for the image inpainting and low-dimensional sets recovery. *Mathematical Methods in the Applied Sciences.* 2017;40(10):3637–3650.

19. Belhachmi Zakaria, Kallel Moez, Moakher Maher, Theljani Anis. WEIGHTED HARMONIC AND COMPLEX GINZBURG-LANDAU EQUATIONS FOR GRAY VALUE IMAGE INPAINTING.. *International Journal of Numerical Analysis & Modeling.* 2016;13(5).

20. Belhachmi Z., Hecht F.. An adaptive approach for the segmentation and the TV-filtering in the optic flow estimation. *Journal of Mathematical Imaging and Vision.* 2016;54(3):358–377.

21. Belhachmi Z., Bernardi C., Karageorghis A.. Mortar spectral element discretization of nonhomogeneous and anisotropic Laplace and Darcy equations. *M2AN.* 2007;41:801–824.

22. Belhachmi Z., Hecht F.. Control of the effects of regularization on variational optic flow computations. *Journal of Mathematical Imaging and Vision.* 2011;40(1):1–19.

23. Ambrosio L., Tortorelli M.. On the approximation of free discontinuity problems. *Boll. Un. Mat. Ital..* 1992;6:105–123.

24. Braides A.. *Gamma-Convergence for Beginners*. No. 22in Oxford Lecture Series in Mathematics and Its Applications. Oxford University Press; 2002.

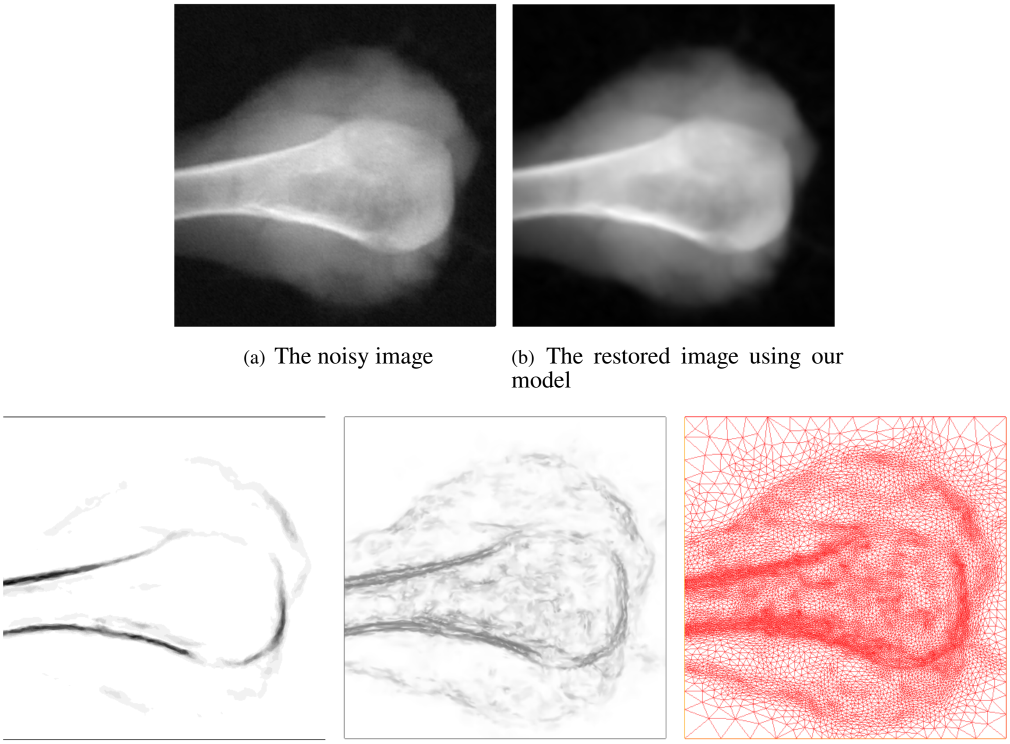

(a) The noisy image (b) The restored image using our model

(c) The map of $\alpha(\cdot)$ (d) The map of $\beta(\cdot)$ (e) The adapted mesh

**FIGURE 4** Our model solved by Augmented Lagrangian and ADMM: Example of medical image denoising and edges detection.

25. Boyd Stephen, Parikh Neal, Chu Eric, Peleato Borja, Eckstein Jonathan. Distributed Optimization and Statistical Learning via the Alternating Direction Method of Multipliers. *Machine Learning*. 2010;3(1):1–122.

26. Wang Yu, Yin Wotao, Zeng Jinshan. Global convergence of ADMM in nonconvex nonsmooth optimization. *Journal of Scientific Computing*. 2019;78(1):29–63.

27. Glowinski Roland. *Lectures on numerical methods for non-linear variational problems*. Springer Science & Business Media; 2008.

28. Goldstein Tom, O'Donoghue Brendan, Setzer Simon, Baraniuk Richard. Fast alternating direction optimization methods. *SIAM Journal on Imaging Sciences*. 2014;7(3):1588–1623.

29. Eckstein Jonathan, Yao Wang. Augmented Lagrangian and alternating direction methods for convex optimization: A tutorial and some illustrative computational results. *RUTCOR Research Reports*. 2012;32(3).

30. Nishihara Robert, Lessard Laurent, Recht Benjamin, Packard Andrew, Jordan Michael I. A general analysis of the convergence of ADMM. *arXiv preprint arXiv:1502.02009*. 2015;.

31. Chan Stanley H, Wang Xiran, Elgendy Omar A. Plug-and-play ADMM for image restoration: Fixed-point convergence and applications. *IEEE Transactions on Computational Imaging*. 2016;3(1):84–98.

(a) The noisy image (b) **TV**: Restored image, $PSNR = 29.1$ (c) **HOM**: Restored image, $PSNR = 29.08$

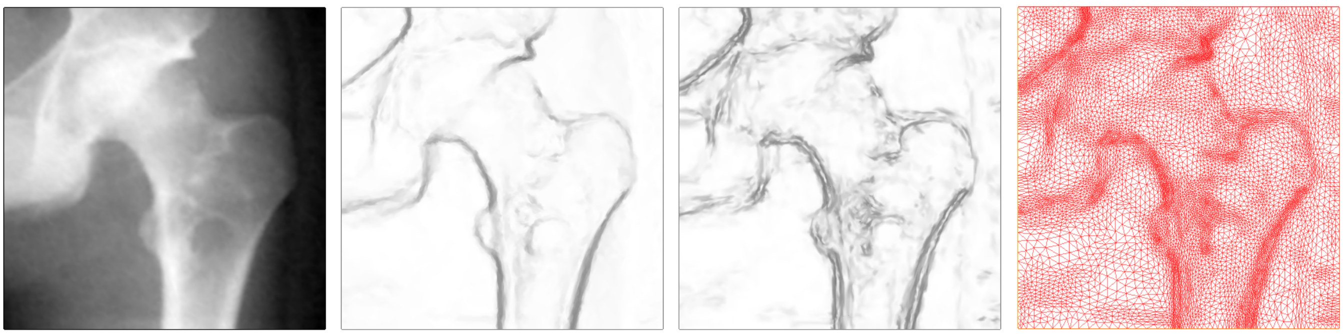

(d) Our model: Restored image, $PSNR = 29.35$ (e) Our model: The map of $\alpha(\cdot)$ (f) Our model: The map of $\beta(\cdot)$ (g) Our model: The adapted mesh

**FIGURE 5** Medical image denoising and edges detection: Comparison between Total variation model (TV), the high-order model (LLT) and our model.